INTERNATIONAL JOURNAL OF INTELLIGENT CONTROL AND SYSTEMS
VOL.15,NO.4,DECEMBER 2010,41-48

Robust Edge Extraction for Swissranger SR-3000 Range Images by Singular Value Decomposition Filtering and Hough Transform

Cang YE and GuruPrasad M. HEGDE

Abstract—**This paper presents a new method for extracting object edges from range images obtained by a 3D imaging sensor–the SwissRanger SR-3000. In the range image pre-processing stage, the method enhances object edges by using surface normal information; and it employs the Hough Transform to detect straight line features in the Normal-Enhanced Range Image (NERI). Due to the noise in the sensor's range data, an NERI contains corrupted object surfaces that may result in unwanted edges and greatly encumber the extraction of linear features. To alleviate this problem, a Singular Value Decomposition (SVD) filter is developed to smooth object surfaces but retain edges. The efficacy of the edge extraction method is validated by experiments in various indoor environments.**

***Index Terms*-Image processing, Hough transform, and edge extraction**

I. INTRODUCTION

Linear structures, such as doorways, stairways and hallways, are ubiquitous in indoor and urban environments. Detection and localization of the linear features are important for mobile robot navigation. This paper concerns reliable detection and localization of linear features in a range image. Since linear features appear as edges in a range image, we call the detection and localization of these features edge extraction for simplicity. Edge extraction is helpful for robot navigation for three reasons. First, a robot may classify a set of linear features into a stairway, a hallway, or a doorway and build a symbolic world map for its operating environment. Second, tracking and following a horizontal edge (representing hallway or curb line) is a simple and effective behavior in navigation. Third, a doorway / stairway may be used as a waypoint or the target of navigation, i.e., they may serve for way-finding function. For instances, a stair-climbing robot may use a stairway as a waypoint to access the next storey of a building.

Laser Detection and Ranging (LADAR) [1] and stereovision systems [2] have been widely used to collect 3D range data. A LADAR system has a low range data throughput and is good for map building with a stationary platform. If a mobile platform is used, a highly accurate inertial measurement unit is required to register each laser scan into a 3D map. Such a system may be prohibitively costly and therefore unsuitable for many mobile robotic applications. In addition, a LADAR system can be bulky and thus cannot be used in a small-sized mobile platform. A stereovision system needs to match a pixel in one camera to that in another camera and triangulate its depth information. This operating principle limits its use in feature-rich environments. Also, a stereovision system is sensitive to illumination and has low range resolution and accuracy for a distant object.

Recently a new class of 3D ranging sensors has been developed by several groups [3], [4]. These devices are commonly referred to as "Flash LADAR." [5], [6], [7] A Flash LADAR illuminates the entire scene by a modulated light source. Each cell of the imaging sensor can determine the time-of-flight of the modulated signal and thus the depth information of a detected object. These devices do not require a scanning mechanism and can provide dense data points at a high frame rate. Therefore, they are promising for mobile range data acquisition. Due to the use of active vision a Flash LADAR works very well in a featureless environment. This is an apparent advantage over stereovision systems.

In this work, we investigate the feasibility of using a Flash LADAR—the SwissRanger SR-3000 [8] for mobile robot navigation in indoor environments. Figure 1a depicts the miniature SR-3000 sensor and Fig. 1b is a snapshot taken from our experiment to calibrate the SR-3000 using data from a LADAR—Sick LMS 200. As a preliminary step we target at edge extraction of those commonly occurring linear structures, such as stairways, doorways, and hallways from the SR-3000's range images. These linear structures are edges in the form of long straight line segments in a range image. In general, edges in a range image need to be enhanced for reliable extraction. In the literature, surface normal [9], [10] has been used for edge enhancement. The normal-based enhancement method is straightforward as an edge is the intersection of two planes having different normals. In a noise-free condition extracting edges from the enhanced range image is trivial: the Hough Transform (HT) would be sufficient. Unfortunately, range data acquired by a Flash LADARs are usually noisy. In particular, the SR-3000's

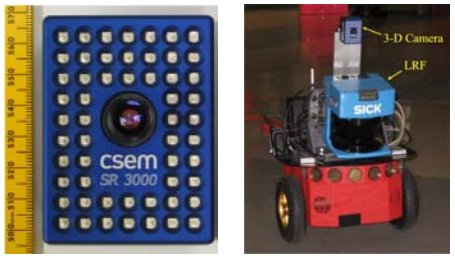

(a) The SR-3000 sensor (b) SR-3000 on the robot

Fig.1 The SR-3000 and LADAR mounted on the Pioneer P3-DX robot: the SR-3000 is much smaller in size. (LRF: LADAR)

This work was supported in part by NASA and the Arkansas Space Grant Consortium under grants UALR17800, UALR18800, and a NASA EPSCoR RID Award.

C. Ye and G. Hegde are with the Department of Applied Science, University of Arkansas at Little Rock, Little Rock, AR 72204, USA (phone: 501-683-7284; fax: 501-569-8020; e-mail: cxye@ualr.edu and gmhegde@ualr.edu).

sensing technology is nascent and its range data has relatively large measurement errors (much bigger than that of a LADAR [11]) due to random noise (e.g., thermal noise and photon short noise) and environmental factors (e.g., surface reflectivity). A normal-based edge enhancement method is very sensitive to noise in range data. As a result it corrupts the object surfaces while enhancing the edges. The corruption may result in large amount of unwanted edges and deteriorate the HT's efficiency in linear feature extraction.

In this paper we study the effect of the SR-3000's range noise on range image enhancement and the HT-based edge extraction, and develop a method to alleviate the ill effect of the noise. The remainder of the paper is organized as follows: In Section II we introduce the SR-3000 imaging sensor. In Section III we discuss the ill effect of range noise on normal-based range image enhancement and the HT–based edge extraction. In Section IV we briefly explain the principle of the Singular Value Decomposition (SVD) filtering method. In Section V we introduce our SVD filter for noise removal. Section VI presents experimental results and the paper is concluded in Section VII.

II. THE SWISSRANGER SR-3000

The state-of-the-art imaging sensor SR-3000 is developed and manufactured by MESA Imaging. It is a CMOS sensor and is capable of capturing 3D range data in real time. The camera has a physical dimension of 50×48×65 mm^3 and a field of view of 47.5×39.6 degrees. It uses 55 infrared LED (wavelength: 850 nm) for illumination. The light source is amplitude modulated. The sensor has a non-ambiguity range of 7.5 meters (due to the 20 MHz modulation) and a spatial resolution of 176×144 pixels. Each pixel is capable of demodulating an optical wave impinging on the sensor by a lock in pixel method [12]. The amplitude and phase shift of the reflected light are used to determine the intensity and distance information of a target point. Therefore, the camera delivers both intensity and range image for each captured frame.

The sensor's error in range measurement is affected by various environmental factors such as surface reflectivity and target distance in addition to the intrinsic factors such as noise of the CMOS sensor and the driving electronics [12]. This paper addresses the possibility of reducing the effect of the error on range data processing.

III. EFFECT OF RANGE ERROR ON IMAGE ENHANCEMENT AND EDGE EXTRACTION

A range image encodes image pixels' depth information as gray values. In case of small depth contrasts, some object edges may be indistinctive. This is demonstrated in Fig. 2b—a range (depth) image obtained by the SR-3000 in the environment shown in Fig. 2a. The box's bottom edge disappears in the floor. For this reason, object edges need to be enhanced for proper extraction. In this work we adopt the method in [10] for range image enhancement. We first represent a set of range data by a tri-band color image where each pixel's RGB values represent the *x* and *y* components of the surface normal $\vec{N}_p = [n_x, n_y, n_z]$ and depth information *Z* of the corresponding point. The color coding is given by:

$$\begin{cases} R = k_1 \cos^{-1} n_x \\ G = k_2 \cos^{-1} n_y \\ B = k_3 Z \end{cases}, \quad (1)$$

where k_1, k_2 and k_3 are positive constants that maintains the R/G/B values in [0, 255]. We then convert the tri-band image into a gray image that we called a Normal-Enhanced Range Image (NERI). It should be noted that: (1) the use of *x* and *y* components is sufficient to represent the surface normal since $n_z = \sqrt{1 - n_x^2 - n_y^2}$; (2) the row and column indices and the blue component (i.e., the Z value) of a tri-band image pixel fully determines the 3D coordinates of the corresponding data point. This means that the scheme encodes a 3D point's local geometric information (surface normal) and global information (location) into a pixel in the NERI.

Figure 2c shows the NERI of Fig. 2b. It can be observed that the box's edges are enhanced but the surfaces are corrupted. To evaluate the level of surface corruption, we obtain the edge image (Fig. 2d) by running the Sobel edge detector (using a threshold of 8) on the NERI. It is noted that throughout this paper an edge image is obtained in the same way, unless otherwise specified. It can be seen that the

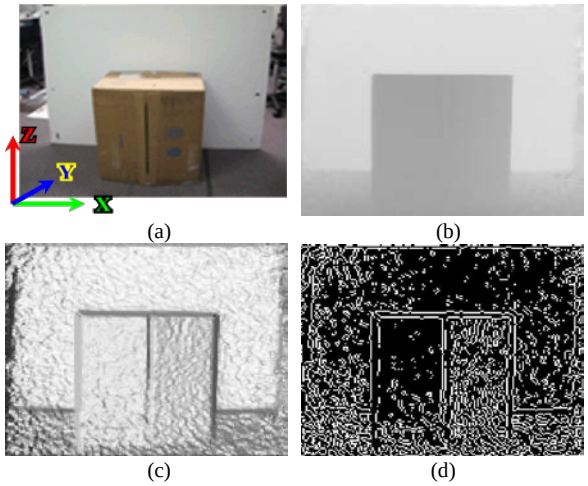

Fig. 2 Normal-based range image enhancement: (a) Actual scene, (b) Range image from the SR-3000, (c) NERI, (d) Edge image of (c).

corruption creates a lot of unwanted tiny edges in the edge image. These tiny edges may result in incorrect linear feature detection when the HT is applied.

The main advantages of the HT are its robustness to image noise and discontinuities of pattern [13], [14]. The tolerance to discontinuous pattern may cause problem to edge extraction in our case. As can be seen in Fig. 2d, the tiny edges contain a large amount of collinear pixels that may be detected by the HT as a straight line if their votes in the same accumulator cell

(in the Hough parameter space) accumulate to a certain level. Figure 3 depicts the straight lines (in green) detected by the HT on the edge image in Fig. 2d. Apparently, the HT detected many false lines. One may argue that the false lines can be removed in a post-processing stage by examining the pixel discontinuities. The problem is that the true object edges may also be discontinuous due to the imperfection of the edge detector. This makes the post-processing unserviceable. It is therefore desired to develop a filtering method that may smooth the object surfaces in a NERI (i.e., to reduce the

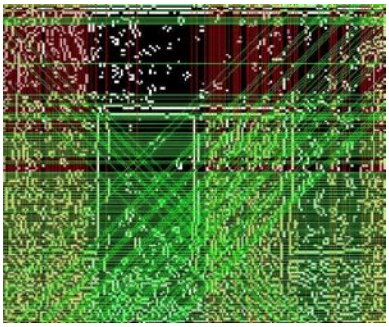

Fig. 3 Lines detected by the HT on the NERI's edge image

amount of tiny edges in the corresponding edge image) but preserve the object edges. In this work, we develop a filtering method based on the Singular Value Decomposition (SVD) to smooth a NERI.

IV. THE SVD FOR NOISE REDUCTION

A. Image Reconstruction by the SVD

SVD and Eigen vector analysis are classical tools used in digital image processing [15]. An $M\times N$ image can be denoted by matrix $\mathbf{A}=[a_{ij}]$ for $i=1, \ldots, M$ and $j=1, \ldots, N$. The SVD of matrix $\mathbf{A}$ takes the following form

$$\mathbf{A} = \mathbf{U}\mathbf{S}\mathbf{V}^T = \sum_{i=1}^{R} s_i \mathbf{u_i} \mathbf{v}_i^T , \qquad (2)$$

where the orthogonal matrices $\mathbf{U}$ and $\mathbf{V}$ consists of the left and right singular vectors $\mathbf{u_i}$ and $\mathbf{v_i}$, i.e., $\mathbf{U}=(\mathbf{u_1}, \ldots, \mathbf{u_M})$ and $\mathbf{V}=(\mathbf{v_1}, \ldots, \mathbf{v_M})$. $\mathbf{U}$ and $\mathbf{V}$ are of order $M\times M$ and $N\times N$, respectively. $\mathbf{S}$ is a $M\times N$ matrix where the diagonal elements s_i for $i=1, \ldots, R$ are the nonnegative singular values of $\mathbf{A}$ and all off-diagonal elements are zero. s_i are arranged in a non-increasing order, i. e., $s_1 \geq s_2 \geq \ldots \geq s_R \geq 0$, in matrix $\mathbf{S}$. If the rank of $\mathbf{A}$ is $R \leq min(M, N)$, then $s_i>0$ for $i=1, \ldots, R$ and $s_i=0$ for $i=R+1, \ldots, N$. The SVD of $\mathbf{A}$ indicates that an image can be restored as the weighted sum of a set of R base images $\mathbf{B_i} = \mathbf{u_i}\mathbf{v_i^T}$ for $i=1, \ldots, R$. The singular value s_i represents the contribution of the i^{th} base image $\mathbf{B_i}$ to the reconstruction of image $\mathbf{A}$. The contributing matrix/image of $\mathbf{B_i}$ is $\mathbf{C_i}=[c_{pq}]=[s_i u_{pi} v_{qi}]$ for $p=1, \ldots, M$ and $q=1, \ldots, N$, where u_{pi} and v_{qi} are the element of $\mathbf{u_i}$ and $\mathbf{v_i^T}$, respectively. The energy of image $\mathbf{C_i}$ can be computed by:

$$E_i = \sqrt{\sum_{p=1,\cdots,M}^{q=1,\cdots,N} c_{pq}^2} \qquad (3)$$

Since $\mathbf{u_i}$ and $\mathbf{v_i}$ are unit vectors, we have

$$E_i = s_i \sqrt{\sum_{p=1,\cdots M} \left(u_{pi}^2 \sum_{q=1,\cdots,N} v_{qi}^2 \right)} = s_i \sqrt{\sum_{p=1,\cdots M} u_{pi}^2} = s_i \qquad (4)$$

This means that s_i represents the energy of image $\mathbf{C_i}$. The decreasing order of s_i in matrix $\mathbf{S}$ implies that the energy of the i^{th} base image decreases as i approaches R. In general, a small number of base images are sufficient to represent the original image although a larger number of base images may add more image details. This property of the SVD has been used in image compression or coding.

Figure 4 illustrates the SVD-based image reconstruction using different Number of Base Images (NBI). The intensity image of the scene (Fig. 4a) is obtained by the SR-3000. Since the SR-3000 has a spatial resolution of 176×144 pixels, the SVD process results in 144 base images. Figure 4g depicts the original image (NBI=144). The reconstructed images with the NBI of 3, 15, 45, and 84 are shown in Fig. 4b, c, d and e, respectively. It can be seen that image reconstruction is not possible with too fewer base images due to excessive loss of image information. However, using too many base images may result in an unnecessarily large file size but does not substantially improve image quality. This can be interpreted from the energy point of view: the base images corresponding to the main image features possess large energy while those corresponding to image details have much smaller energy.

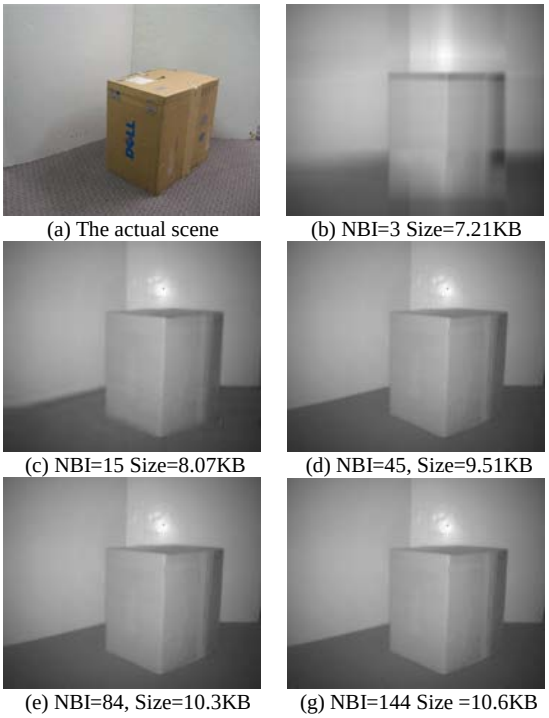

(a) The actual scene (b) NBI=3 Size=7.21KB
(c) NBI=15 Size=8.07KB (d) NBI=45, Size=9.51KB
(e) NBI=84, Size=10.3KB (g) NBI=144 Size =10.6KB

Fig. 4 Image reconstruction using different NBI: the image with NBI=45 is satisfactory in term of image details and file size.

B. The SVD Filtering

A noise-free image **A** has a lower rank ε, $\varepsilon<min(M, N)$ [1]. The SVD in Eq. 2 produces the following singular values in a non-increasing order: $s_1 \geq s_2 \geq s_3 \geq \ldots \geq s_\varepsilon > s_{\varepsilon+1} = \ldots = s_{min(M,N)} = 0$. A noisy image can be described by matrix $\mathbf{D}=\mathbf{A}+\mathbf{\Delta}$, where $\mathbf{\Delta}$ is a noise perturbation matrix. Generally, matrix **D** has a full rank $R=min(M, N)$ [16], i.e., all singular values are nonzero. This means that the last $R-\varepsilon$ base images are mostly related to additive noise. Usually, the image to be filtered has good signal to noise ratio, meaning that the energy of the image components is much larger than that of the noise. Therefore, the last $R-\epsilon$ singular values, $s_{\varepsilon+1}, \ldots$, and s_R, are much smaller than the preceding ones. By eliminating the singular values $s_{\varepsilon+1}, \ldots$, and s_R, we may obtain the noise-free image without losing image details. This property is demonstrated by Fig. 5 that is the intensity image constructed by the last 99 base images. It can be viewed as the complement image of Fig. 4d. Fig. 5 mostly contains noise while Fig. 4d contains sufficient image content.

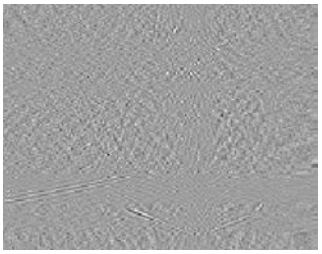

Fig. 5 Complement image of fig. 4d

Figure 6 exemplifies the noise removal capability of the SVD filtering method. A computer-generated noise-free image (Fig. 6a) is used in this case study. The edge image of Fig. 6a is shown in Fig. 6b. Figure 6a is corrupted by Gaussian noise to obtain the image in Fig. 6c whose edge image is depicted in Fig. 6d. It can be seen that the Gaussian noise results in many pepper-like edges in the edge image (Fig. 6d) and some corruptions in the edges of the two rectangular objects. Figure 6e is the reconstructed image by Eq. 2 (using the first four singular values). The result in noise reduction is satisfactory by comparing Fig. 6e with the original image (Fig.6a). This is also supported by the edge image (Fig. 6f) that is close enough to the original edge image (Fig. 6b).

In this example we use ε=4 to filter the noise and reconstruct the image as the rank of the original noise-free image is four. However, in practice the value of ε is not a priori known for an image to be filtered. It is therefore desired to estimate the optimal value for ε with which the SVD filtering method achieves a good trade-off between image detail retention and noise removal. In [16] a block-based SVD filtering method is proposed to remove noise in an intensity image. The method exploits the fact that random noise is much harder to compress compared with image data (ordered information). It determines the value of ε by the following steps: (1) reconstruct an intensity image using Eq. 2 by nullifying the last k singular values; (2) perform a lossless compression on the resultant image and record the image file size $F(k)$; and (3) plot $F(k)$ against $log(k)$, and ε locates at the knee point of the curve. It is noted that a knee point is the point where the second derivative reaches its maximum. In [17] a similar approach is used to filter random noise from deterministic data. We have attempted to use the same method to filter an NERI. We found that the SVD filter itself worked very well but the method proposed in [16] for determining ε didn't work in our case. We suspect that it is because the corruption in the NERI does not appear to be random noise. Based on our experiments on various environments, we find that it is possible to determine ε for the SVD filter by simply analyzing the singular values. The SVD filter with such a value of ε works pretty well. Unlike the method in [16], [17], our approach does not need to analyze the reconstructed images and is thus very computationally efficient.

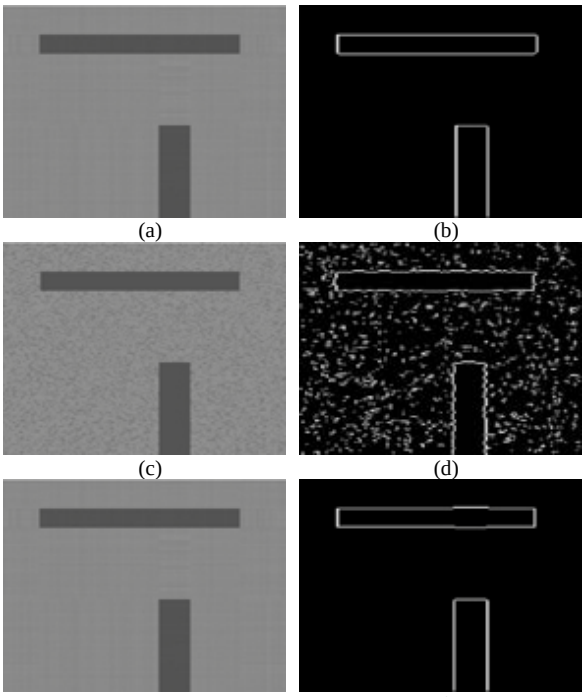

Fig. 6 Noise reduction by the SVD filter: (a) Computer-generated, noise-free image (size: 176×144), (b) Edge image of (a), (c) Image corrupted by Gaussian noise, (d) Edge image of (c), (e) Reconstructed image with the first four singular values, (f) Edge image of (e).

V. THE PROPOSED METHOD

As we have seen in Section IV, the value of ε determines the quality of the reconstructed image. By using a good estimation of ε to reconstruct the NERI, we should be able to retain the image details and remove the majority of the noise. Eventually, we can extract the true edges of the linear structures by applying the HT on the edge image. In this section, we present our proposed filtering method and describe how we extract the edges in an NERI.

We first construct the NERI and then perform the SVD (Eq. 2) on the NERI. Since the matrix of the NERI is 176×144 and it has full rank due to noise, we have 144 singular values, s_i for i=1, …, 144, that are arranged in a non-increasing order. The plot of s_i against i shows that the singular values drop drastically with increasing i (see Fig. 9 for an example). The curve stays flat when i is sufficiently big. In other words, the first derivatives of the singular values initially have negatively big values, and they rapidly approach zero with increasing i (Fig. 10). This property holds true in all of our experiments with various scenes. This can be explained from the energy point of view. More distinctive and larger features (e.g., long edges) in a NERI possess higher energy and thus have larger singular values. Less distinctive and smaller features have smaller singular values due to their lower energy levels. Surface corruptions look like tiny image details and have the lowest energy level. Therefore, their singular values are very small. The rapid decrease of the singular values suggests that we may readily determine the value of ε by setting a threshold to the curve of the first derivative.

Our SVD filtering method for NERI is carried out as follows:

1) Construct the NERI and obtain the singular values, s_i for i=1, …, 144, of the NERI matrix.
2) Normalize s_i by $\bar{s}_i = s_i / \max(s_i)$ and compute the first derivatives $\bar{s}_i' = d\bar{s}_i / di = d\bar{s}_i$ for i=1, …, 143.
3) The value K that satisfies $\bar{s}_m' > \delta$ for m=K, K+1, …, 143 is recorded. Here, δ is a threshold value that is empirically determined by experiment. In this study δ=0.001. The threshold value for the SVD filter is then determined as $\varepsilon=K+1$.
4) Set the last 144-ε singular values to zero, i.e., s_i=0 for i=ε+1, …, 144, and reconstruct the NERI using Eq. 2.

Once the noise in the NERI is reduced, we apply the HT to the filtered NERI's edge image to detect straight lines. The edges are then extracted and projected back onto the original range image. With the known pose of the imaging sensor, the location of these linear structures can be easily determined.

To demonstrate the efficacy of the filtering method, we apply the filter to the NERI in Fig. 2c. The resultant NERI is

(a) The filtered NERI (b) Edge image (c) Detected linear edges

Fig.7 The filtered NERI and linear edges detected by the HT

shown in Fig. 7a that indicates a great reduction in surface corruption. The edge image is much cleaner than that in Fig. 2d. By applying the HT on Fig. 7b, we obtain a smaller number of detected straight lines (Fig. 7c) that represents the true edges of the objects.

VI. Experiments and Results

We have validated our edge extraction method in various indoor environments. Currently, our method is implemented in Matlab 7.7 on a computer with an AMD Phenom 9950 Quad-core Processor (2.60 GHz), 4 GB RAM, and Window Vista OS. The results of five experiments are shown in Fig. 8, 12, 13, 14 and 15. The 1st experiment demonstrates edge extraction of a doorway (Fig. 8). Figure 8 shows the different stages from creating the NERI to extracting edges of the doorway. We can see from the results that the filter results in a much smoother NERI (Fig. 8d). It then becomes feasible to extract the true edges of the doorway (Fig. 8f) that are along the red and green lines (Fig. 8e) detected by the HT.

Figures 9 and 10 depict the plots of the singular values and the first derivative for this experiment, respectively. We can see a drastic decrease in the magnitudes of the first few

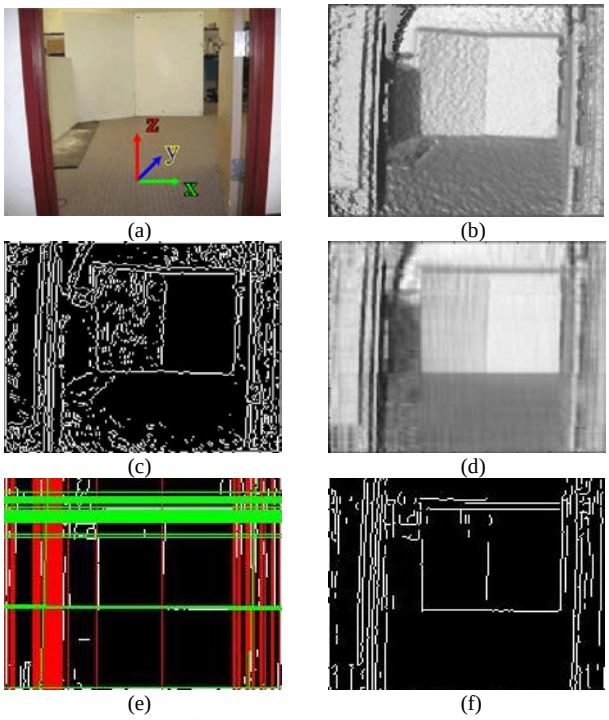

Fig. 8 Edge extraction for a doorway environment: (a) Actual scene, (b) NERI of (a), (c) Edge image of (b), (d) The filtered NERI, (e) Hough lines superimposed on the edge image of (d), (f) Extracted edges.

singular values. The first derivatives of the singular values rapidly approach zero. In this example the most significant singular value is 24816. Thus δ is set around -24 (0.001 if normalized) and ε is found to be 12. It is noted that the curves are plotted using the actual singular values to show their true magnitudes. Figure 11 depicts the magnified view of segment AB in Fig. 10 that demonstrates oscillation of the curve. The way that we determine ε value (step 3 of the SVD filtering) skips unstable segment of the curve and ensures that the rate of change of singular values is sufficiently small after ε.

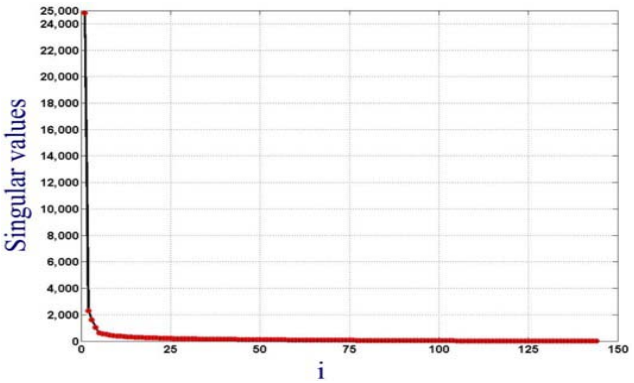

Fig. 9 Plot of the Singular values (s_i) versus i

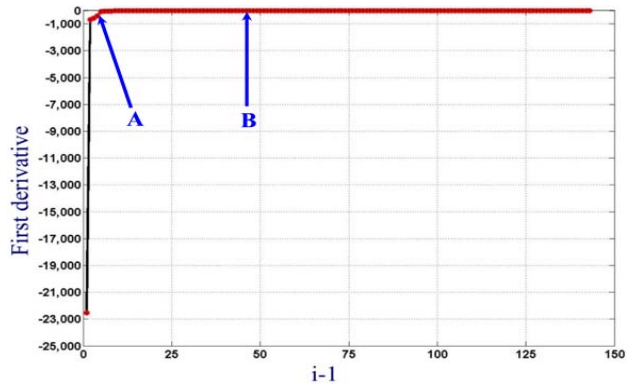

Fig. 10 Plot of the first derivatives of the Singular Values

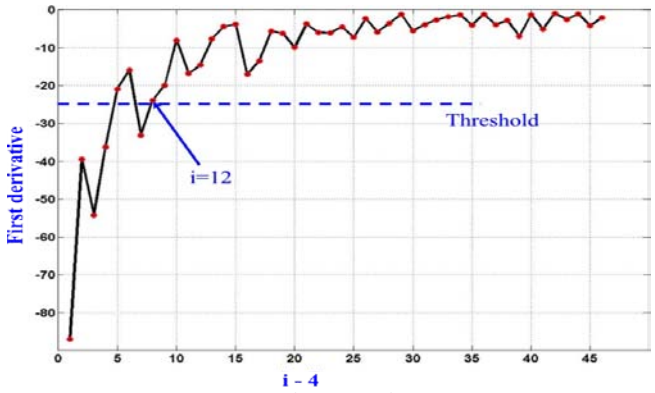

Fig. 11 Magnified view of segment AB

The 2nd experiment shows edge extraction of a stairway. The results are displayed in Fig. 12. The method works efficiently and extracts the straight line segments of the steps. In this case, the range measurement errors cause relatively larger corruption to the NERI (Fig. 12b). This can also be observed from Fig. 12c where a large number of tiny edges clutter in the edge image. It is not possible for the HT to detect the edges of the steps from this edge image. The filter removes majority of the corruption and produces a decent filtered NERI (Fig. 12d). The resultant edge image contains almost no tiny edges and leads to the extraction of the linear edges of steps.

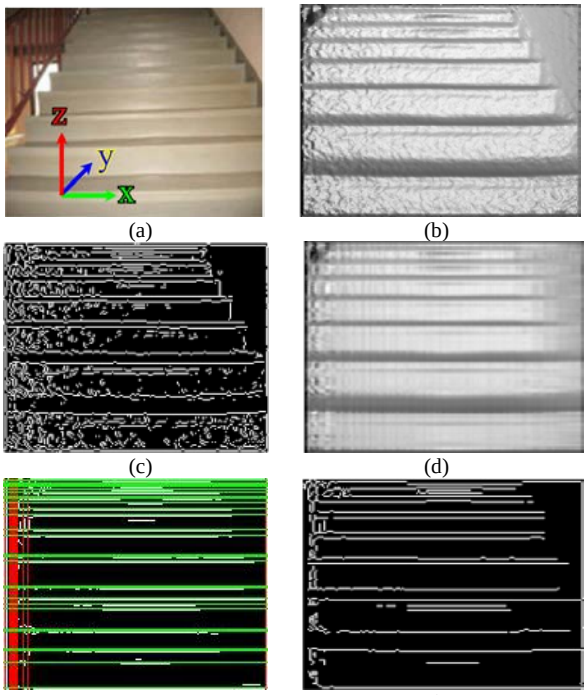

Fig. 12 Edge extraction of a stairway (ε=8): (a) Actual scene, (b) NERI, (c) Edge image of (b), (d) The filtered NERI, (e) Hough lines superimposed on the edge image of (d), (f) Extracted edges.

Figure 13 shows the results of the experiment in a cluttered laboratory environment consisting of a shelf and a toolbox rack. The results demonstrate satisfactory filtering and edge extraction performance of the proposed method.

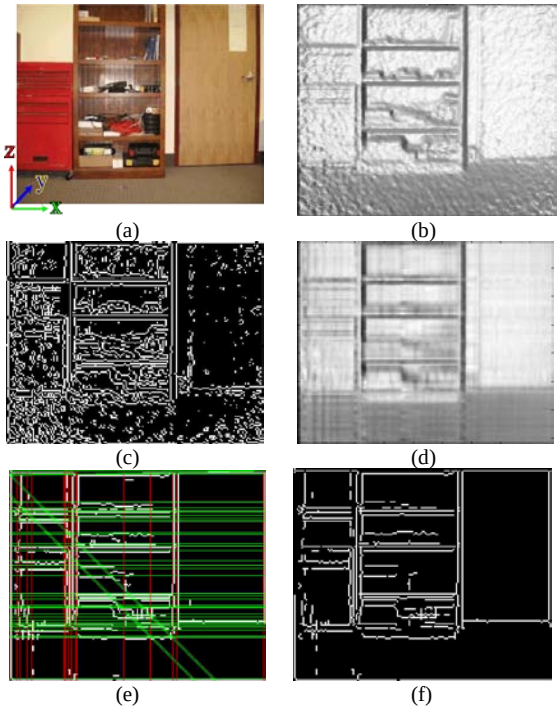

Fig. 13 Edge extraction of laboratory environment (ε=9): (a) Actual scene, (b) NERI of (a), (c) Edge image of (b), (d) The filtered NERI, (e) Hough lines superimposed on the edge image of (d), (f) Extracted edges.

Experiments five and six validate the method in the cases of a scene with a dust can (Fig. 14) and a scene with 4 vertical poles (Fig. 15). Table I summarizes the results of the five experiments. The experimental results indicate: (1) A small number of base images are sufficient for reconstructing an NERI; (2) The filtering method is computationally inexpensive; (3) The executing time of the HT line detection depends on the complexity of the NERI (number of straight line edges) and it may take ~21 seconds. Currently, the method is implemented in Matlab. The computational time can be substantially reduced if the code is written in C++ language.

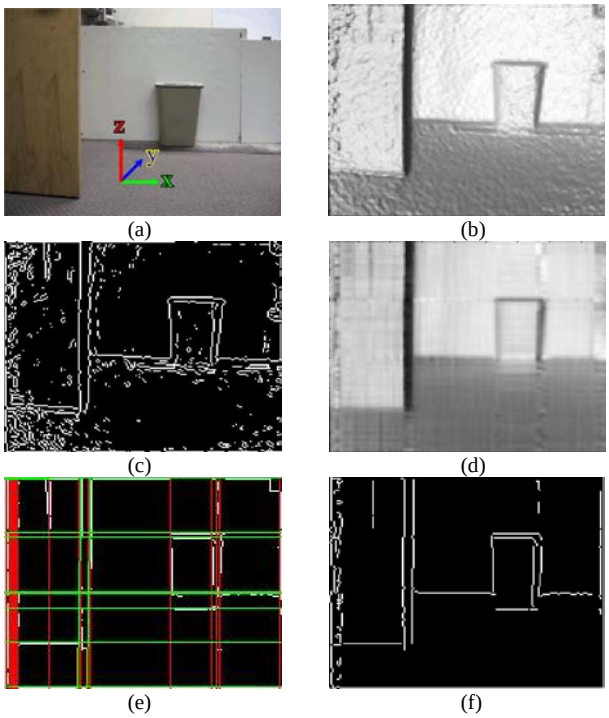

Fig. 14 Edge extraction of a trash can (ε=8): (a) Actual scene, (b) NERI of (a), (c) Edge image of (b), (d) The filtered NERI, (e) Hough lines superimposed on the edge image of (d), (f) Extracted edges.

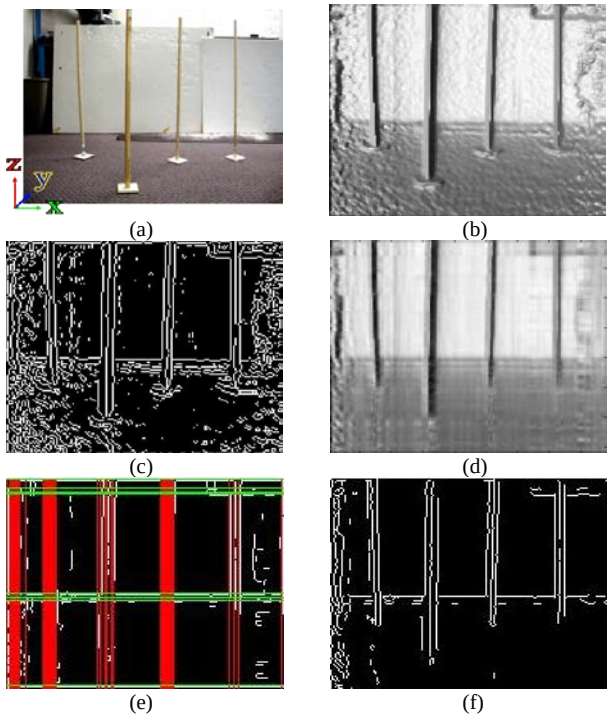

Fig. 15 Edge extraction of a scene with vertical poles (ε=*10*): (a) Actual scene, (b) NERI of (a), (c) Edge image of (b), (d) The filtered NERI, (e) Hough lines superimposed on the edge image of (d), (f) Extracted edges.

TABLE I SUMMARY OF THE EXPERIMENTAL RESULTS

Scene	Figure	Max. SV	Threshold (ϵ)	SVD filtering time (seconds)	HT time (seconds)
Doorway	8	24816	12	0.0513	19.674
Staircase	12	28111	8	0.0459	21.157
Lab	13	28834	9	0.0454	19.253
Trash can	14	27787	8	0.0456	9.329
Poles	15	26506	10	0.0465	16.169

SV: Singular Values

VII. Conclusions

We have presented a method that may reliably extract the edges of linear structures from the range images captured by the SwissRanger SR-3000. In the proposed method, surface normal information is used for edge enhancement and to transform a range image into an NERI. To alleviate the ill effect of the accompanying surface corruption, we propose a filtering method based on the SVD. The filter can effectively remove the surface corruption but retain image details without requiring prior knowledge of either the NERI or the characteristics of the surface corruption (range errors). The filter is computationally inexpensive and it enables the Hough Transform to reliably extract the linear edges from the NERI. We have validated the method's efficacy by experiments in various environments.

We will extend this method to the extraction of curved object edges in our future work. The method can be employed by a mobile robot for autonomous navigation.

References

[1] C. Ye, "Navigating a mobile robot by a traversability field histogram," *IEEE Transactions on Systems, Man, and Cybernetics-Part B: Cybernetics*, vol. 37, no. 2, pp. 361-372, 2007.

[2] R. Turchetto and R. Manduchi, "Visual curb localization for autonomous navigation," in *Proc. IEEE/RSJ International Conference on Intelligent Robots and Systems*, 2003, pp. 1336-1342.

[3] http://www.3dvsystems.com

[4] http://www.canesta.com

[5] R. Stettner, H. Bailey, and R. D. Richmond, "Eyesafe laser radar 3d imaging," in *Proc. SPIE, vol. 4377 of Laser Radar Technology and Applications*, September, 2001.

[6] R. Gvili, A. Kaplan, E. Ofek and G. Yahav, "Depth key," *SPIE Electronic Imaging Conference*, Santa Clara, California, 2003.

[7] S. B. Gktürk, H. Yalcin, and C. Bamji, "A time-of-flight depth sensor - system description, issues and solutions," in *Proc. IEEE Computer Society Conference on Computer Vision and Pattern Recognition Workshops*, 2004, pp. 35-35.

[8] T. Oggier, B. Büttgen,F. Lustenberger, "SwissRanger SR3000 and first experiences based on miniaturized 3D-TOF Cameras," *Swiss Center for Electronics and Microtechnology (CSEM) Technical Report*, 2005.

[9] K. Pulli, "Vision methods for an autonomous machine based on range imaging," Master's Thesis, University of Oulu.

[10] K. Pulli, M. Pietikainen, "Range image segmentation based on decomposition of surface normals," in *Proc. 8th Scandinavian Conference on Image Analysis*, 1993, pp. 893-899.
[11] C. Ye and J. Borenstein, "Characterization of a 2-D laser scanner for mobile robot obstacle negotiation," in *Proc. IEEE International Conference on Robotics and Automation*, 2002, pp. 2512-2518.
[12] T. Oggier, et al., "An all-solid-state optical range camera for 3D real-time imaging with sub-centimeter depth resolution," in *Proc. SPIE*, vol. SPIE-5249, pp. 534-545, 2003.
[13] M. Atiquzzaman, "Multiresolution Hough transform-an efficient method of detecting patterns in images," *IEEE Transactions on Pattern Analysis and Machine Intelligence*, vol. 14, no. 11, pp. 1090 – 1095, 1992.
[14] A. Y. S. Chia, *et al.*, "Ellipse Detection with Hough Transform in One Dimensional Parametric Space," in *Proc. IEEE International Conference on Image Processing*, 2007, pp. V333-V336.
[15] H. C. Andrews and C. L. Patterson, "Singular value decompositions and digital image processing," *IEEE Transactions on Acoustics, Speech, and Signal Processing*, vol. ASSP-24, pp. 26–53, 1976.
[16] K. Konstantinides, B. Natarajan, and G. S. Yovanof, "Noise estimation and filtering using block-based singular value decomposition," *IEEE Transactions On Image Processing*, vol. 6, no. 3, pp. 479-483, 1997.
[17] B. K. Natarajan, "Filtering random noise from deterministic signals via data compression," *IEEE Transactions on Signal Processing*, vol. 43, no.11, pp. 2595–2605, 1995.

Guruprasad M Hegde received B.E. degree from Sardar Vallabhbhai National Institute of Technology, India in June 2005. He is currently working towards a PhD in Engineering Science and Systems at the University of Arkansas at Little Rock, AR. He is a student member of IEEE and his current research interests include range image segmentation and robot navigation.

Cang Ye received B.E. and M.E. degree from the University of Science and Technology of China, P. R. China in 1988 and 1991, respectively. He received his Ph.D. degree from the University of Hong Kong in 1999.

He is currently an Associate Professor in Department of Applied Science, University of Arkansas at Little Rock, AR. He was a research investigator at University of Michigan, Ann Arbor, MI from 2003 to 2005. His research interests are in mobile robotics, robotic assistive technology, fuzzy systems and reinforcement learning.

Dr. Ye is a senior member of IEEE and a member of Technical Committee on Robotics and Intelligent Sensing, IEEE Systems, Man, and Cybernetics Society.